Supporting Information

Grigorova et al. 10.1073/pnas.1009968107

SI Materials and Methods

Confocal Microscopy. Peripheral LNs were fixed in 4% paraformaldehyde solution in PBS for 2 h and then incubated in 30% sucrose solution in PBS overnight. Ten- to 30-μm cryostat sections were stained with various combinations of antibodies, including rat mAbs to LYVE-1 clone 223322 (R & D Systems) conjugated to Alexa Fluor 488 (A488) or Alexa Fluor 647 (A647), anti-CD4 mAb conjugated to phycoerythrin (PE) or to A647 (RM4-5; BD Pharmingen), anti-CD19 mAb conjugated to PE, primary Armenian hamster anti-CD31 (Thermo Scientific) mAb, and secondary anti-Armenian hamster mAb conjugated to Cy5. Images were acquired on an SP2-AOBS or an SL confocal microscope (Leica Microsystems), using the 488-, 594-, and 633-nm laser lines to excite A488 (and CFSE), Texas Red (and CMTMR and PE), and A647, respectively. Emission slits were tuned to 498–550 nm for Alexa Fluor 488, to 604–625 nm for Texas Red, and to 650–700 nm for Alexa Fluor 647. Confocal images were processed using MetaMorph software (Molecular Devices) and Adobe PhotoShop CS2.

3D Reconstruction of LYVE-1$^+$ Sinuses, HEVs, and T-Cell Area in ILN. LNs were isolated from C57BL/6 mice 12 h after injection of 20 μg of anti-LYVE1 (A488) s.c. in the flanks and tail base. Sequential 20- to 30-μm cryostat sections of ILNs were collected. Sections from some sequentially cut ILNs were stained with anti-CD4 (A647). In these sections HEVs were weakly stained with anti-LYVE-1 (A488). Alternatively, sections from sequentially cut ILN were stained with primary Armenian hamster anti-CD31 mAb, secondary anti-Armenian hamster mAb (Cy5), and anti-CD4 (PE). *Z* stacks of every ILN section were collected with confocal imaging and were tiled together using Leica Microsystems software. The images were collected with a 20× objective (Δ*xy* resolution, 1.46 μm). Sequential *z* stacks were processed to remove the out-of-focus planes and then aligned using MetaMorph (Molecular Devices) software to build a 3D reconstruction of an ILN lobe. Representative ILN (541 *z* planes at ∼1.06 μm apart) reconstruction was then processed in Imaris 6.4.2 × 64 (Bitplane) software to assign polygons matching to all LYVE-1$^+$ sinuses, HEVs, and T-cell areas in every *z* plane of the reconstruction, using an Imaris polygon-drawing tool. 3D surfaces of the T zone and all cortical sinuses and HEVs were then created in Imaris and exported into MatLab (MathWorks). Confocal analysis of the CD4 T-cell shape index inside and outside of the blunt-ended sinuses was performed using MetaMorph in two 3D reconstructed ILNs (four different blunt-ended structures in each were analyzed). The long and short axes of the cells were measured at every 10th *z* plane containing a blunt-ended region via the line segment. Cell shape indexes were then calculated as the ratio of the longer axis to the shorter axis.

Footpad (FP) and s.c. Administration of HEL-A647 and HEL-PE and Their Detection in the LNs. For detection of HEL-A647 (molecular mass ∼14 kDa) localization in LNs, purified MD4 and MD4 CXCR5 B cells were labeled with CMTMR. In some experiments MD4 CXCR5 B cells were simultaneously colabeled with CMTMR and CFSE. Labeled cells (10^7 to 2×10^7 per mouse) were injected i.v. 40 h before HEL administration. HEL-A647 appearance in the LNs was studied when HEL-A647 was administered into the FP (∼0.3 μg, 10 μL of PBS) for 2, 5, and 10 min. For visualization of HEL-PE (molecular mass ∼300 kDa) localization in LNs, unlabeled MD4 and MD4 CXCR5$^{-/-}$ splenocytes were transferred into recipients by i.v. injection (∼10^8 total cells per mouse) after lysis of the red blood cells. HEL-PE appearance in the LNs was studied when HEL-PE was administered into the FP (0.3–0.4 μg, in 10 μL of PBS) for 3 min or s.c. into flanks and the base of the tail to drain to ILNs (3–4 μg, in 120 μL of PBS) for 30 and 40 min. After the FP and s.c. injections, peripheral, draining popliteal, and inguinal LNs were isolated correspondingly at the times indicated and were fixed and processed for section analysis. Sections were stained with anti-LYVE-1 (A488). To detect the unlabeled MD4 and MD4 CXCR5$^{-/-}$ cells, LN sections were stained with HEL-A647 (0.03 μg/μL, 1,000 dilution). Colocalization of CMTMR-labeled MD4/MD4 CXCR5$^{-/-}$ cells with Alexa 647 signal (for HEL-A647 injections) and A647-labeled MD4/MD4 CXCR5$^{-/-}$ cells with PE signal (for HEL-PE injection) inside and outside of LYVE-1$^+$ sinuses was assessed by confocal microscopy.

Studies of Lymphocyte Localization into LYVE-1$^+$ Sinuses. To assess when lymphocytes could localize into the cortical LYVE-1$^+$ sinuses, T and B cells were purified from C57BL/6 mice, labeled with CMTMR and the CMTMR/CFSE combination correspondingly, and injected i.v. into recipient mice ($1–1.5 \times 10^7$ cells of each kind) for 20 or 30 min. Peripheral LN sections were stained with anti-LYVE-1 (A488) and anti-CD31 (Cy5) as described above and analyzed by confocal microscopy. To assess lymphocyte displacement from the cortical LYVE-1$^+$ sinuses after poly(I:C) treatment, CD69$^{-/-}$ and CD69$^{+/+}$ lymphocytes (B or T cells) were isolated from CD69$^{-/-}$ and C57BL/6 mice, labeled with CMTMR and CFSE correspondingly, and transferred i.v. into recipient mice ($1–1.5 \times 10^7$ cells of each kind). Forty hours after the transfer, recipient mice were injected with 100 μg of poly(I:C) or PBS (i.v.). Peripheral LNs were isolated 6 h later and sections were stained with anti-LYVE-1 (A647) mAb and analyzed by confocal microscopy. To enumerate CD69$^{-/-}$ and CD69$^{+/+}$ cells inside and outside the sinuses, at least 10 thick sections with LYVE1 sinuses were analyzed for each LN. [CD69$^{+/+}$ ↦ WT] and [CD69$^{-/-}$ ↦ WT] BM chimeras were injected i.v. either with 100 μg of poly(I:C) or with PBS. Six hours after treatment peripheral LNs were isolated and sections were stained with anti-LYVE-1 (A488), anti-CD4 (A647), and anti-CD19 (PE) mAbs and analyzed by confocal microscopy. Analysis was performed on three mice treated with poly(I:C) and two mice treated with PBS for each of the BM chimeras.

Studies of CD69 Up-Regulation Kinetics in Locally Inflamed LNs. To induce localized LN inflammation 30 μL of poly(I:C) (5 μg) was injected into the FP with simultaneous injection of PBS into the contralateral FP. Ly5.2 lymphocytes were isolated from C57BL/6 mice and transferred ($4–6 \times 10^7$ cells) i.v. into Ly5.1 recipient mice at 6 or 18 h after the poly(I:C) injection. Twenty minutes after cell transfer, lymphocyte entry into LNs was blocked by i.v. injection of 30 μg of anti-α_4 and -α_L mAb. At various times after that, the poplitieal LNs were isolated and the cells were stained by fluorochrome-conjugated anti-CD69 mAb (H1.2F3; BD Pharmingen) and analyzed by FACS. The experiment at 6 h after poly(I:C) injection was repeated three times and that at 18 h after after poly (I:C) injection one time.

Intravital Microscopy and Two-Photon Imaging. Intravital and explanted ILN preparation and imaging were performed as described (1). To label LYVE-1$^+$ structures in vivo 12–18 h before intravital microscopy, recipient mice were injected s.c. in the flank and tail base with 20 μg of the mAb LYVE-1 conjugated to Texas

Red to drain to both medial and lateral lobes of the inguinal lymph node. GFP$^+$ T cells or B cells ($2–4 \times 10^7$) were transferred into recipient mice 12 h before imaging. Deep tissue images were acquired with a custom-built two-photon microscope as described (1) or with an LSM 7 MP microscope (Zeiss). A MaiTai TiSapphire laser (Spectra-Physics) or Chameleon Ultra II (Coherent) was tuned to provide an excitation wavelength of 870 nm to image Texas Red and GFP. In experiments with the LSM 7 MP microscope, images were collected with objective *W* "*Plan-Apochromat*" 20×/1.0 (Zeiss). Emission wavelengths of 470–510 nm (second harmonic emission of collagen fibers), 525–575 nm (CFSE, GFP, and Alexa Fluor 488) and 605–675 nm (CMTMR, PE, and Texas Red) were collected with nondescanned detectors (Zeiss).

Two-Photon Image Processing and Data Analysis. Images were acquired with Video Savant (IO Industries) or with Zen 2009 (Zeiss) software. Maximum intensity time-lapse images were generated with Imaris 6.4.2 × 64. Videos were processed with a low pass noise filter. Cell tracks, 3D rotation images, and LYVE-1$^+$ structure reconstructions were made with Imaris 6.4.2 × 64 and Imaris 5.01 × 64. In some movies, drift of the imaging volume was corrected by Imaris software. Automated tracks of T cells were verified and corrected manually. GFP cell localization relative to the outside, inside, and border of the cortical LYVE-1$^+$ sinuses was determined using Imaris software on the basis of the manual assessment of the relative position and colocalization of the fluorescent signal between the T-cell and LYVE-1$^+$ structures in every *z* plane containing cell images for every time point. Volume rendering of LYVE-1$^+$ structures was performed using manual surface creation tools in Imaris software. Entry frequency was defined as the ratio of T-cell commitments to go inside the sinus starting at the outer border of the sinus vs. total number of times that cells left the outer border. The entry frequency was separately calculated for cells arriving at the outer border of the sinuses from parenchyma or from within the sinuses. The time periods spent by T cells at the outer border of LYVE-1$^+$ sinuses were separately calculated for cells transmigrating into the sinuses and for cells returning into parenchyma. To calculate T-cell entry frequencies and distribution of T-cell time at the outer border, >175 events were analyzed from four experiments previously described (1). Annotation and final movie compilation were performed in Adobe After Effects 7.0. Movie files were converted to mpeg format with Avi to Mpeg Converter for Windows 1.5 (FlyDragon Software).

Model of Antigen Diffusion Against the Flow. ***Model design.*** To evaluate whether it was feasible for a high molecular weight antigen to get into the cortical sinus by diffusion against the direction of flow, we designed a simple model of protein diffusion and convection. Antigen spreading was simulated in a 3D region, a cylinder 300 μm long with a 30-μm diameter (Fig. S2*A*) representing a cortical sinus. The model had three dependent variables: flow velocity vector $\vec{v}$, pressure p, and antigen concentration c. The independent variables were coordinates x, y, z, and time t. Lymph was assumed to be an incompressible viscous fluid; presence of cells was neglected. Stationary approximation for flow was used to describe flow velocity and pressure by time-independent Navier–Stokes equations:

$$\rho\cdot\left(\vec{v}\cdot\vec{\nabla}\right)\vec{v} = -\vec{\nabla}p + \mu\cdot\Delta\vec{v} \qquad \text{[S1]}$$

$$\left(\vec{\nabla}\cdot\vec{v}\right) = 0. \qquad \text{[S2]}$$

Antigen was assumed to freely diffuse in the volume. Transient (i.e., time-dependent) diffusion and convection were considered. The equation for the antigen concentration was therefore a basic mass transport equation:

$$\frac{\partial c}{\partial t} = D\Delta c - \left(\vec{v}\cdot\vec{\nabla}c\right). \qquad \text{[S3]}$$

The initial condition assumed no antigen in the cortical sinus:

$$c|_{t=0} = 0. \qquad \text{[S4]}$$

Boundary conditions on the sinus wall were no-slip conditions for fluid and no-permeability conditions for the antigen. We thus neglected binding of antigen and did not consider permeability of the walls:

$$\vec{v} = \vec{0} \qquad \text{[S5]}$$

$$\left(\vec{n}\cdot\vec{\nabla}c\right) = 0. \qquad \text{[S6]}$$

Boundary conditions on the outlet were set to zero pressure, no viscous stress, and constant antigen concentration:

$$\left(\nabla\vec{v} + (\nabla\vec{v})^T\right)\cdot\vec{n} = \vec{0} \qquad \text{[S7]}$$

$$p = 0 \qquad \text{[S8]}$$

$$c = c_0. \qquad \text{[S9]}$$

Boundary conditions on the inlet were set to nonzero pressure (sufficient to create flow with velocities similar to the experimentally observed ones), no viscous stress, and nonpermeability for the antigen:

$$\left(\nabla\vec{v} + (\nabla\vec{v})^T\right)\cdot\vec{n} = \vec{0} \qquad \text{[S10]}$$

$$p = p_0 \qquad \text{[S11]}$$

$$\left(\vec{n}\cdot\vec{\nabla}c\right) = 0. \qquad \text{[S12]}$$

This set of differential equations was numerically integrated using COMSOL Multiphysics software in the combination of stationary incompressible Navier–Stokes and transient convection-diffusion modes.

Model parameters. The following parameter values were used unless specified otherwise: cylinder length L_x, 300 μm; cylinder diameter L_{yz}, 30 μm; simulation time t_{max}, 30 min; fluid density ρ, 1,000 kg/m^3; fluid dynamic viscosity μ, 0.0016 Pa × s; diffusion coefficient D, 4×10^{-7} cm^2/s = 4×10^{-11} m^2/s; pressure difference p_0, 8×10^{-4} Pa; and antigen concentration in the subcapsular sinus c_0, 10 nM.

Simulation results. The solution for flow velocity was time-independent, a typical Poiseuille parabola with the maximal velocity of 9.4×10^{-8} m/s ~ 5.7 μm/min achieved on the cylinder axis (Fig. S2*B*). To model HEL-PE (~300 kDa) distribution, a diffusion coefficient of 4×10^{-7} cm^2/s was selected, on the basis of diffusion coefficients measured for proteins with distinct molecular weights (2). Antigen with $D \sim 4 \times 10^{-7}$ cm^2/s efficiently diffused in this system (Fig. S2*C*). Within 3 min, it was effectively spread across one-third of sinus length (blue line in Fig. S2*D*) and, within 30 min, its concentration in the blunt end of the cortical sinus became ~60% of that in the subcapsular sinus (Fig. S2*D*, red line). With flow velocity variation, diffusion efficiency changed inversely: If the velocity was increased by an order of magnitude, the antigen concentration achieved in the blunt end of the sinus was decreased approximately by the same factor (Fig. S2*E*).

These data suggest that it is indeed possible for a high molecular weight antigen to spread by diffusion upstream of the sinus in the presence of flow velocities with rates on the order of tens of

micrometers per minute. Curiously, diffusion efficiency was strongly impaired with the diffusion coefficient decrease (Fig. S2*F*). For example, for a virus with a diffusion coefficient of ~4×10^{-8} cm^2/s (4×10^{-12} m^2/s) (3, 4), concentration in the upper end of the cortical sinus was by a few orders of magnitude smaller than for an antigen having a diffusion coefficient that was only 10-fold greater (Fig. S2*F*, *Inset*).

Development of Quantitative Model of T-Cell Egress from Inguinal Lymph Node (ILN). ***Model parameters.*** To build a quantitative model of T-cell egress from ILNs, the following parameters were measured experimentally: (*i*) lymphocyte motility within the T zone, (*ii*) the distribution of lymphocyte entry (HEVs) and exit (LYVE-1^+ sinuses) sites with respect to the T-cell areas in ILN, and (*iii*) frequency of T-cell transmigration into the exit sites upon contact:

i. Parameters describing T-cell motility were obtained on the basis of six independent TPLSM experiments imaging cortical T cells in ILNs. T cell trajectories, obtained by Imaris software, were then used to calculate the correlation time of T-cell random walk, $<\tau_{corr}>$ (5), and the average squared displacement, $<\Delta R^2>$ vs. time (Fig. S5*A*).

ii. Images of LYVE-1^+ cortical sinuses, HEVs and CD4 T cells were obtained as described in *SI Materials and Methods* by confocal microscopy of ILN serial sections. Images from a representative ILN were aligned using Metamorph software to build a complete 3D reconstruction of a single lobe (Fig. 1*A* and Movie S1). Every *z* stack of the reconstruction was then processed in Imaris software to fit T-zone area and each of the structures to a matching polygon (Fig. S5 *B–E*). Polygon labeling of the LYVE-1^+ sinuses outlines sinus regions that are not densely filled with LYVE-1^+ signal inside (LYVE-1^+ macrophages). Polygon labeling of HEVs is defined by $CD31^{hi}$ and LYVE-1^{lo} sinuses with high endothelial cell morphology. Polygon labeling of the T zone is defined as the regions densely filled with CD4-positive cells of rounded morphology. Coordinates of the polygons outlining the T zone and all cortical sinuses and HEVs were then exported into Matlab. Note that only HEVs and LYVE-1^+ sinuses polygons within the T-zone polygon were used as a 3D volumetric framework for the in silico T-cell migration.

iii. The average frequency of T-cell transmigration into LYVE-1^+ cortical sinuses upon contact was calculated on the basis of the quantitative analysis of migration in relation to the cortical sinuses of ILNs in four independent TPLSM experiments (1) (Fig. S5*F*). These quantitative studies were performed using mature thymocyte transfers because they involved comparisons of wild-type and $S1P_1$-deficient T cells, and the latter cells do not emigrate from the thymus. The transferred thymocytes present in the LNs had a mature CD4 and CD8 single positive T-cell phenotype.

Models of T-cell random walk. i. Simple model. To generate T-cell trajectories in silico that would possess random walk characteristics ($<\tau_{corr}>$ and $<\Delta R^2>$ vs. time) of T-cell migration within the LNs, we first used a simple model of random walk (SM), previously suggested for modeling lymphocyte migration (6). The SM of random walk generates trajectories with a fixed period of straight movement followed by entirely random change of direction. To approximate T-lymphocyte random migration, duration of the straight motion in the SM was fixed to the experimentally measured $<\tau_{corr}>$ = 2.7 min, and velocity of movement was varied to fit $<\Delta R^2>$ vs. time of the trajectories generated in silico to the values measured experimentally (Fig. S6*A*, gray circles). To preserve trajectories within a constrained volume (T zone, outside of LYVE-1^+ sinuses), when coordinates of the generated trajectory would lie outside the volume, a new 2.7-min step with entirely random angle would be generated (Fig. S6*B*).

ii. Conditional probability model. In the SM of random walk the curvy trajectories of T-cell migration are approximated by fixed periods of straight motion (Fig. S6*B*). Although good for reproducing displacement of the T-cell population, this approximation may result in reduction of the overall path of T cells, thus reducing their volume-sampling characteristics. In addition, the SM may be inaccurate for describing T-cell movement at the border of restricted volumes (LYVE-1^+ sinuses). Therefore, we developed a conditional probability model (CPM) that is based on cell "memory" of its previous trajectory and should be better at approximating the curvy pattern of T cell-correlated random walk. For generation of the CPM we analyzed trajectories from six independent experiments (in each experiment ≥60 tracks, each track ≥10 min, with Δt = 20-s step interval). From each trajectory the 20-s step sequence of apparent velocities (v), angles (α), and plane angles (θ) was extracted to calculate the distribution of conditional probabilities for parameters (v, α, and θ) of the next step depending on the parameters of the previous step(s) (Fig. S6 *C* and *D*). CPM random walks were generated in silico, where every 20-s step was generated randomly but according to the calculated conditional probability distributions. The CPM random walk with a memory of a few various preliminary steps was tested to find the best combination that would fit the experimentally obtained average random walk characteristics ($<\tau_{corr}>$ and $<\Delta R^2>$ vs. time) (Fig. S6*E*). The CPM with two-step memory and the following combination of conditional probabilities, $P(v_2/v_1)$, $P(\alpha_{12}/v_1)$, $P(v_3/v_1, v_2, \alpha_{12})$, $P(v_3/v_1, v_2, \alpha_{12})$, $P(\theta_1/v_1, v_2, \alpha_{12})$, showed a good fit to the experimentally determined $<\tau_{corr}>$ and $<\Delta R^2>$ vs. time and was used in further calculations. To preserve trajectories within constrained volumes (T zone, outside of LYVE-1^+ sinuses), when the coordinates of the generated trajectory would lay outside the volume, a new 20-s step would be generated randomly according to the conditional probabilities distribution.

T-cell exit model algorithm. All simulations were performed using software written in Matlab. 3D volumetric data of ILN T zone, HEVs, and LYVE-1^+ cortical sinuses were exported into Matlab and used as a framework for the in silico T-cell migration. Starting (entry) T-cell positions were selected by generating random points on HEV polygons within the T-zone area. Random movement of T cells was modeled either by SM or by CPM algorithms. At each micrometer of the generated trajectories, coordinates of the trajectories were assessed for their containment within the T zone and proximity to the lymphatic sinuses. Contact and minimal distances to the LYVE-1^+ sinuses were assigned in each simulation to account for the finite volume of the cells. When the distance between coordinates of the in silico T-cell and LYVE-1^+ cortical sinuses was equal or less than the contact distance (CD), the in silico cell was registered as "in contact" with the sinuses. When coordinates were closer than an assigned minimal distance (MD) to the lymphatic sinus or were outside of the T-cell area, a new random walk step was generated instead of the last micrometer displacement of the previous step. (Fig. S6 *B* and *F*). Duration of each generated trajectory was at least 15 h in silico time unless the trajectory went into the second lobe of ILN, and the track history was stopped. For each condition 500 tracks were generated. Statistics of T-cell contacts with LYVE-1^+ cortical sinuses (Fig. 6 *A* and *B*) and the experimentally measured frequency of T-cell transmigration into sinuses upon contact (Fig. S5*F*) were used to calculate the probability of T-cell transmigration into the cortical sinuses at various times after entry into ILN. The latter calculations were repeated 10,000 times to overcome limited statistics of the 500 tracks, and median values were taken (Fig. 6 *C* and *D*). Less than

2% of tracks ended in the second lobe before their first collision with LYVE-1$^+$ cortical sinuses, and <4% before their calculated transmigration into LYVE-1$^+$ cortical sinuses.

Comparison between the simple and conditional probability models. The 20% shorter half-life for T-cell transmigration into the sinuses predicted by the CPM algorithm compared with the SM algorithm (Fig. 6 *C* and *D*) is due to both faster initial contacts with the sinuses (Fig. 6 *A* and *B*) and shorter time intervals between consecutive contacts with LYVE-1$^+$ cortical sinuses (~6 vs. 8 min difference between the CPM and the SM). These differences may be due to higher sampling of LN volume by the CPM algorithm compared with the SM algorithm. In addition, upon encounter with LYVE-1$^+$ sinus walls in silico, T-cell trajectories generated by the CPM tend to preserve correlated movement along the sinuses, whereas in the SM a new entirely random direction is generated. This new direction results in significantly longer LYVE-1$^+$ sinus contact time calculated by the CPM compared with the SM (Fig. S6 *G–J*). A fairly good agreement of the LYVE-1$^+$ sinus contact time, calculated by the CPM (with CD = 5 μm, MD = 2 μm), with the values measured experimentally (1) (Fig. 2*D*), may also suggest that the overall correlated random walk characteristics describing T cell motility may be sufficient to explain T-cell movement along the sinus border, and no additional mechanism for T-cell retention at the sinuses has to be evoked.

Sensitivity of the SM exit model to CD and MD. Because our exit model does not take into account cell size and shape, we varied contact and minimal distance to assess how sensitive the exit model is to these parameters. Decreasing the CD from 5 to 3 μm had only a small effect on the rate of first encounters with the sinuses (Fig. 6 *A* and *B*) and the calculated half-life of T cells in ILNs (Fig. 6*C*, Fig. S7*A*). Similarly, changing the MD from 2 to 0 μm did not lead to a significant change in T-cell transit time (Fig. S7*A*). However, when the contact distance was not taken into account, the calculated half-life of T cells was ~1.5-fold longer (Fig. S7*A*). Therefore, incorporation of the contact distance into the model is important for estimation of cell residence time in ILN, although the model is not very sensitive to CD variations within the physiological range (between 3 and 5 μm).

Sensitivity of the SM to HEVs. Because most of the LYVE-1$^+$ cortical sinuses run in proximity to HEVs, we asked whether encounters of T cells with HEVs could reduce access of the T cells to the cortical sinuses. To address this, in silico trajectories of T cells were prevented from "going through" HEVs. To do that, when T-cell distances to HEV were <2 μm (MD = 2 μm), new random walk steps were generated. This modification did not significantly increase the calculated half-life of T cells in the ILNs, suggesting that HEV avoidance does not have to be incorporated into the model (Fig. S7*A*).

Sensitivity of the SM to variation in V and $<\tau_{corr}>$. To calculate how sensitive the SM is to variation in the velocity and time of its correlated walk we first calculated the range of velocities (with a fixed $<\boldsymbol{\tau}_{\mathbf{corr}}>$) and the range of $<\boldsymbol{\tau}_{\mathbf{corr}}>$ (with fixed average V) that would cover variation in $<\Delta\mathbf{R}^{\mathbf{2}}>$ vs. time that was determined experimentally in six different T-cell imaging experiments (Fig. S6*A*). Corresponding variation of velocity ($V \pm 14\%$) and the time of correlated movement ($<\boldsymbol{\tau}_{\mathbf{corr}}> \pm 22\%$) had <17% effect on the calculated T-cell half-life (Fig. S7*B*).

Volumetric Analysis. Half-lives of T cells in peripheral LNs, experimentally measured by blocking cell entry into the LNs and monitoring the decrease in cell numbers (7), were similar to half-lives measured by other approaches (8). Therefore, using the volumetric analysis, we calculated half-lives for T cells in ILN for situations when cell entry is blocked and under an assumption that all cells transmigrating into sinuses leave the LN. Two extreme cases were evaluated: when the area of the sinus wall does not change upon the decrease in the LN volume (*I*) and when this area linearly depends on the LN volume (*II*). In a more realistic scenario, T cell half-life should lie somewhere in between the two calculated cases.

Assumption: rate of egress is determined by the number of lymphocytes in contact with the LYVE-1$^+$ sinuses and the fraction of lymphocytes that transmigrates through the sinuses per min.

υ^T_{entry}, rate of T-cell entry into inguinal lymph node (ILN);
k, rate constant of T-cell exit from ILN;
$\tau_{1/2}$, half-life of T cells in ILN;
N^T, number of T cells in ILN;
N^T_0, number of T cells in ILN at $t = 0$;
V^T_0, volume of T zone and interfollicular areas in ILN at $t = 0$;
C^T, average concentration of T cells in T zone and interfollicular areas;
N^T_{trans}, number of T cells transmigrating into LYVE-1$^+$ sinuses per minute;
N^T_{LYVE1}, number of T cells in contact with LYVE-1$^+$ sinuses;
V^T_{LYVE1}, volume of the cell layer that is in contact with LYVE-1$^+$ sinuses;
F, fraction of N^T_{LYVE1} that transmigrates into LYVE-1$^+$ sinuses per minute,

$$F = \frac{\sum_{\Delta\tau} \frac{In(\tau_b)}{\tau_b}}{\sum_{\Delta\tau} In(\tau_b) + Out(\tau_b)} \cong \mathbf{0.26}, \text{ where}$$

$$\tau_b = \left[\frac{1}{3}\right], \left[\frac{2}{3}\right], 1, \frac{4}{3}, \frac{5}{3}, \ldots 10(\text{min}) \qquad \textbf{[S13]}$$

(Fig. S8 *A* and *B*).
τ_b, time that T cell spends in contact with LYVE-1$^+$ sinus border;
$In(\tau_b)$, number of cells that spend at the LYVE-1$^+$ sinus border time τ_b and transmigrate into the sinus;
$Out(\tau_b)$, number of cells that spend at the LYVE-1$^+$ sinus border time τ_b and turn back into parenchyma;
h_T, average height of lymphocyte layer that touches LYVE-1$^+$ sinuses,
$h_T \cong 5 - 10$ μm (Fig. S8*C*).
For m Z sections of ILN reconstitution and $n(m)$ LYVE-1 polygons in each Z section:
S_{LYVE1}, surface area of all LYVE1 sinuses that are facing T zone and interfollicular area in ILN;
S^i_T, area of T-zone polygon(s) in the ith Z section (Fig. S8*D*);
$L^{j(i)}_{LYVE1}$, perimeter of the jth LYVE-1 polygon in the ith Z section (Fig. S8*D*);
Δz, distance between Z sections,

$$S_{LYVE1} = \left(L^{1(1)}_{LYVE1} + L^{2(1)}_{LYVE1} + \ldots + L^{n(1)}_{LYVE1} + \ldots + L^{1(m)}_{LYVE1} + L^{2(m)}_{LYVE1} + \ldots + L^{n(m)}_{LYVE1}\right) \cdot \Delta z = \mathbf{5.8 \cdot 10^5} \cdot \Delta z\ \mu\text{m}^2 \qquad \textbf{[S14]}$$

$$V^T_0 = \left(S^1_T + S^2_T + \ldots + S^m_T\right) \cdot \Delta z = \mathbf{2.8 \cdot 10^8} \cdot \Delta z\ \mu\text{m}^3 \qquad \textbf{[S15]}$$

$$N^T_{LYVE1} = C^T \cdot V^T_{LYVE1} = C^T \cdot h_T \cdot S_{LYVE1} \qquad \textbf{[S16]}$$

$$N^T_0 = C^T \cdot V^T_0. \qquad \textbf{[S17]}$$

Case I. Rate of Lymphocyte Egress Does Not Depend on the Size of ILN (Determined Only by the Transmigration of the Cells Adjacent to the LYVE-1$^+$ Sinuses into the Sinuses, and Their Concentration at the Sinuses Is Invariant).

$$\frac{dN^T}{dt} = v^{\ T}_{entry} - kN \qquad \text{[S18]}$$

$\frac{dN^T}{dt} = -k$, when lymphocyte entry into LNs is blocked

[S19]

$$N^T(t) = N_0^T - k{\cdot}t \qquad \text{[S20]}$$

$$\tau_{1/2} = \frac{N_0^T}{2{\cdot}k} \qquad \text{[S21]}$$

$$k = N_{trans}^T = N_{LYVE1}^T{\cdot}F \qquad \text{[S22]}$$

$$\tau_{1/2} = \frac{N_0^T}{2{\cdot}N_{LYVE1}^T{\cdot}F} = \frac{V_0^T}{2{\cdot}h_T{\cdot}S_{LYVE1}{\cdot}F} = \frac{928}{h_T} \approx 1.6-3.1 \text{ h.} \qquad \text{[S23]}$$

Case II. Rate of Lymphocyte Egress Is Proportional to the Size of ILN.

$$\frac{dN^T}{dt} = v^{\ T}_{entry} - kN \qquad \text{[S24]}$$

$\frac{dN^T}{dt} = -kN$, when lymphocyte entry into the LN is blocked

[S25]

$$N^T(t) = N_0^T{\cdot}e^{-kt} \qquad \text{[S26]}$$

$$\tau_{1/2} = \frac{\ln(2)}{k}. \qquad \text{[S27]}$$

At $t = 1$ min

$$N^T(1) = N_0^T - \mathrm{N}_{trans}^T = N_0^T{\cdot}e^{-k} \qquad \text{[S28]}$$

$$k = -\ln\left(\frac{N_0^T - N_{trans}^T}{N_0^T}\right) = -\ln\left(\frac{V_0^T - h_T{\cdot}S_{LYVE1}{\cdot}F}{V_0^T}\right) = -\ln\left(1 - \frac{h_T{\cdot}S_{LYVE1}{\cdot}F}{V_0^T}\right) \qquad \text{[S29]}$$

$$\tau_{1/2} = -\frac{\ln(2)}{\ln\left(1 - \frac{h_T{\cdot}S_{LYVE1}{\cdot}F}{V_0^T}\right)} = -\frac{\ln(2)}{\ln\left(1 - \frac{h_T}{1{,}856}\right)} \approx 2.1-4.3 \text{ h.} \qquad \text{[S30]}$$

Summary. T-cell half-lives in the lymph nodes measured experimentally, ~8–9 h (7, 8); T-cell half-lives, predicted by quantitative models, SM ~ 5.1 h, CPM ~ 4.2 h; and T-cell half-lives predicted by volumetric analysis, 1.6–4.3 h.

1. Grigorova IL, et al. (2009) Cortical sinus probing, S1P1-dependent entry and flow-based capture of egressing T cells. *Nat Immunol* 10:58–65.
2. Liu MK, Li P, Giddings JC (1993) Rapid protein separation and diffusion coefficient measurement by frit inlet flow field-flow fractionation. *Protein Sci* 2: 1520–1531.
3. Harvey JD (1973) Diffusion coefficients and hydrodynamic radii of three spherical RNA viruses by laser light scattering. *Virology* 56:365–368.
4. Brune D, Kim S (1993) Predicting protein diffusion coefficients. *Proc Natl Acad Sci USA* 90:3835–3839.
5. Bazant MZ (2001) Topics in Applied Mathematics Lecture Notes for Spring 2001. Lecture 13: Correlation functions. Available at http://math.mit.edu/~bazant/teach/18.325/lectures/. Accessed May 30, 2010.
6. Beauchemin C, Dixit NM, Perelson AS (2007) Characterizing T cell movement within lymph nodes in the absence of antigen. *J Immunol* 178:5505–5512.
7. Pham TH, Okada T, Matloubian M, Lo CG, Cyster JG (2008) S1P1 receptor signaling overrides retention mediated by G alpha i-coupled receptors to promote T cell egress. *Immunity* 28:122–133.
8. Tomura M, et al. (2008) Monitoring cellular movement in vivo with photoconvertible fluorescence protein "Kaede" transgenic mice. *Proc Natl Acad Sci USA* 105:10871–10876.

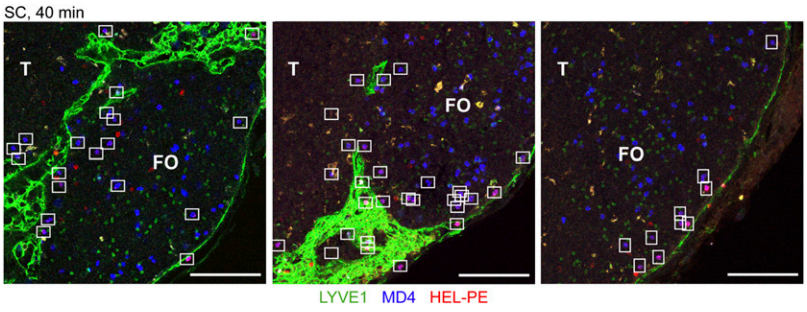

Fig. S1. Emergence of s.c. injected HEL-PE in LNs 40 min after administration. Confocal images of ILN sections are shown, stained to detect LYVE-1 (green) and the transferred MD4 B cells (by HEL-A647, blue) after s.c. injection of HEL-PE into the flanks and the base of the tail. (*Left* to *Right*) Projection views of 13-, 11-, and 14-μm-thick sections. (Scale bars, 100 μm.) Squares indicate MD4 B cells stained with HEL-PE. FO, follicle; T, T zone.

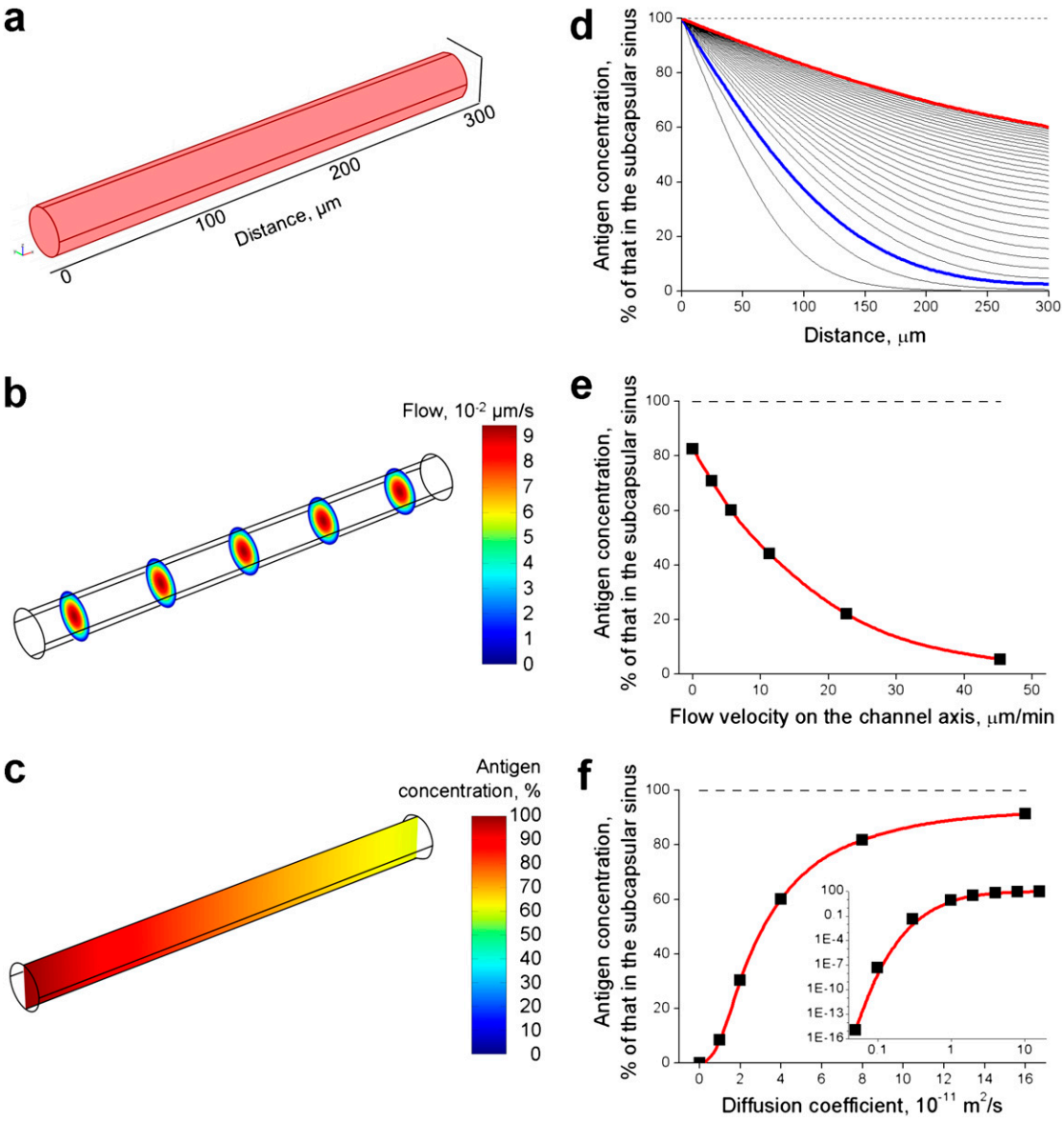

Fig. S2. Diffusion of antigen in the direction opposite to the liquid flow. Dynamic simulations are shown of antigen spreading in the direction opposite to liquid flow. The following parameter values were used as defaults unless specified otherwise: simulation time t_{max}, 30 min; fluid density ρ, 1,000 kg/m^3; fluid dynamic viscosity μ, 0.0016 Pa × s; diffusion coefficient D, 4×10^{-7} cm^2/s = 4×10^{-11} m^2/s; pressure difference p_0, 8×10^{-4} Pa; antigen concentration in the subcapsular sinus c_0, 10 nM. (*A*) Model geometry: The cortical sinus is represented as a cylinder 300 μm long and 30 μm wide. The left facet is the flow outlet and is also the site of contact with the subcapsular sinus, where the antigen concentration is maintained constant. The right facet is assumed to be the flow inlet, corresponding to the blunt end of the cortical sinus. (*B*) Cylinder cross-sections show distribution of flow velocity within the cylinder for default model parameters: It is parabolic, and the maximal (axial) velocity is 9.4×10^{-8} m/s (or ~5.7 μm/min). (*C*) The cross-section shows distribution of the antigen within the cylinder after 30 min for default model parameters. Note that the concentration in the blunt end of the sinus reaches as much as ~60% of that in the subcapsular sinus. (*D*) Distribution of the antigen along the channel axis for different time points up to 30 min. Fluid velocity fixed at 5.7 μm/min and $D = 4 \times 10^{-11}$ m^2/s. Time interval between the lines is 1 min. The thick blue and red lines shows distributions for the 3-min and 30-min time points, respectively. (*E*) Antigen concentration in the blunt end of the cortical sinus as a function of axial flow velocity at the 30-min time point. $D = 4 \times 10^{-11}$ m^2/s. (*F*) Antigen concentration in the blunt end of the cortical sinus as a function of the diffusion coefficient at the 30-min time point. Fluid velocity fixed at 5.7 μm/min. The *Inset* shows the same curve in a double-logarithmic scale.

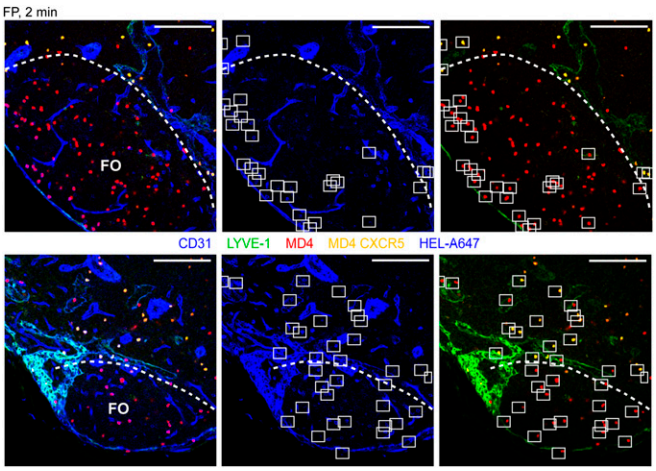

Fig. S3. Emergence of HEL-A647 injected into the footpad in popliteal LNs 2 min after administration. Confocal images are shown of PLN sections with transferred MD4 B cells (red) and MD4 CXCR5$^{-/-}$ B cells (yellow), stained to detect LYVE-1 (green) and CD31 (blue). (*Upper* and *Lower*) Projection view of 17- and 29-μm-thick sections, respectively. (*Left*) Overlay of all colors. (*Center*) Blue color only (CD31 and A647). (*Right*) Red and green colors overlay only (LYVE1, MD4, and MD4 CXCR5$^{-/-}$ B cells). Note some CD31^{+} cells present in follicles. (Scale bars, 100 μm.) Squares indicate MD4 and MD4 CXCR5$^{-/-}$ B cells stained with HEL-A647. Dashed lines approximately outline follicles. FO, follicle.

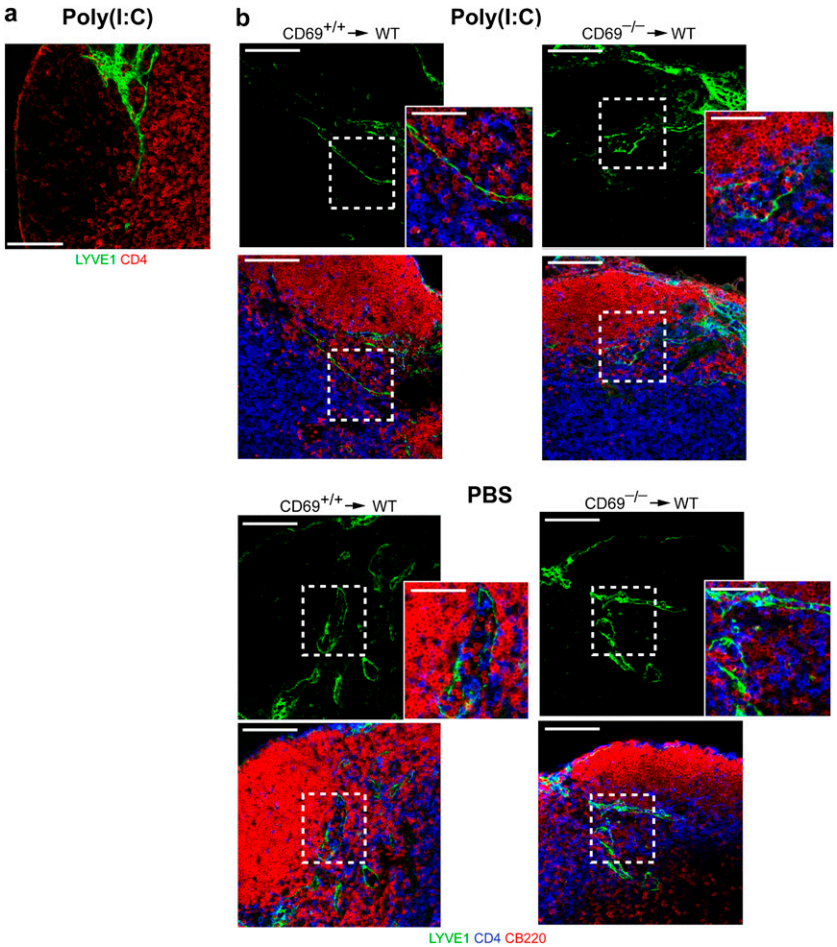

Fig. S4. Collapse of LN cortical sinuses in mice with wild-type but not CD69-deficient lymphocytes during systemic inflammation. (*A*) Confocal image of a peripheral LN section from a WT mouse 6 h after systemic treatment with poly(I:C). Sections are stained with LYVE-1-specific (green) and CD4-specific (red) antibodies. (Scale bar, 100 μm.) (*B*) Confocal images of peripheral LN sections from [CD69$^{+/+}$ ↦ WT] and [CD69$^{-/-}$ ↦ WT] bone marrow (BM) chimeras 6 h after their systemic treatment with poly(I:C) or PBS. The sections are stained with LYVE-1-specific (green), B220-specific (red), and CD4-specific (blue) antibodies. (Scale bar, 100 μm.) (*Insets*) An enlargement of the LYVE-1^{+} cortical sinuses, selected by the dashed squares indicated on the sections. (*Inset* scale bar, 50 μm.) For each type of BM chimera, data are representative of three mice treated with poly(I:C) and two mice treated with PBS.

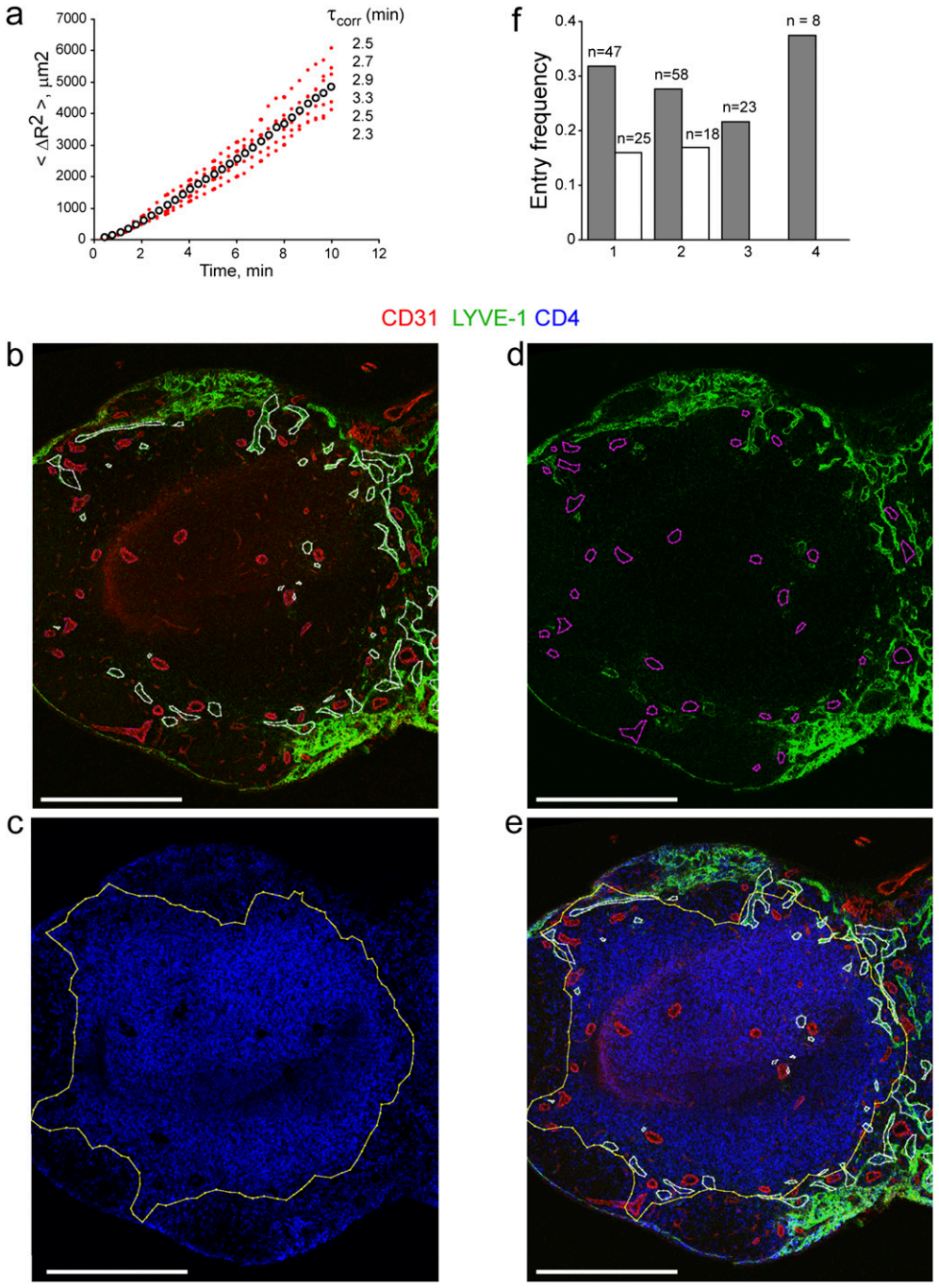

Fig. S5. Parameters of the quantitative model of T-cell egress from ILN. (*A*) Parameters describing T-cell motility in the T zone of ILNs. Plots of the average squared displacement $<\Delta R^2>$ vs. time (red dots) were calculated for six independent TPLSM experiments, imaging migration of T cells in the T zones of explanted ILNs. For each dataset the average time of correlated motion, τ_{corr} was calculated. The above calculations and analysis of T cell trajectories were performed as described in *SI Materials and Methods*. White circles indicate the average $<\Delta R^2>$ vs. time for six experiments (six mice). Average τ_{corr} is 2.7 min. (*B–D*) Delineation of HEV and LYVE-1$^+$ cortical sinus distribution with respect to the T-cell area. Confocal section of ILN (from the serial section analysis) was stained to detect LYVE-1 (green), CD31 (red), and CD4 (blue) and processed in Imaris software to fit the T-zone area and each of the structures of one lobe of ILN to a matching polygon. (Scale bars, 500 μm.) (*B*) Polygon labeling (white line) of the LYVE-1$^+$ sinuses, defined as the sinus regions that are not densely filled with LYVE-1$^+$ signal inside. (*C*) Polygon labeling (yellow line) of the T zone, defined as the region densely filled with CD4-positive cells of rounded morphology. (*D*) Polygon labeling (violet line) of HEVs, defined as CD31^{hi} and LYVE-1^{low} sinuses with high endothelial cell morphology. (*E*) Overlay image of the confocal section with the polygons outlining T-zone polygon (yellow line), LYVE-1$^+$ sinuses (white lines), and HEVs (faint violet lines). Coordinates of the polygons from each section were exported into Matlab to be used as a 3D volumetric framework for the in silico T-cell migration. HEVs and LYVE-1$^+$ sinuses polygons within the T-zone polygon only were considered in the model and the volumetric analysis (*SI Materials and Methods*). (*F*) T-cell entry frequency into LYVE-1$^+$ cortical sinuses upon contact, calculated for four independent TPLSM experiments, on the basis of the quantitative analysis of T-cell migration in relation to the cortical sinuses performed as described in *SI Materials and Methods*. Fraction of T cells approaching LYVE-1$^+$ cortical sinuses from the parenchyma [T zone ↦ Border ↦ Sinus] that transmigrate into the sinuses (gray bar) is shown. The number of events quantified in each experiment is indicated by **n**. The average [T zone ↦ Border ↦ Sinus] entry frequency calculated for two intravital and two explanted ILN imaging experiments is 0.3. The fraction of T cells returning to the outer border of LYVE-1$^+$ cortical sinus from the lumen of sinus that then transmigrates back into the sinus [Sinus ↦ Border ↦ Sinus] (white bar) is shown. The average [Sinus ↦ Border ↦ Sinus] entry frequency calculated for one intravital and one explanted ILN imaging experiments is 0.17. In experiments 3 and 4 frequency of lymphocyte return into the sinuses is not shown, because of the low number of events (n = 3).

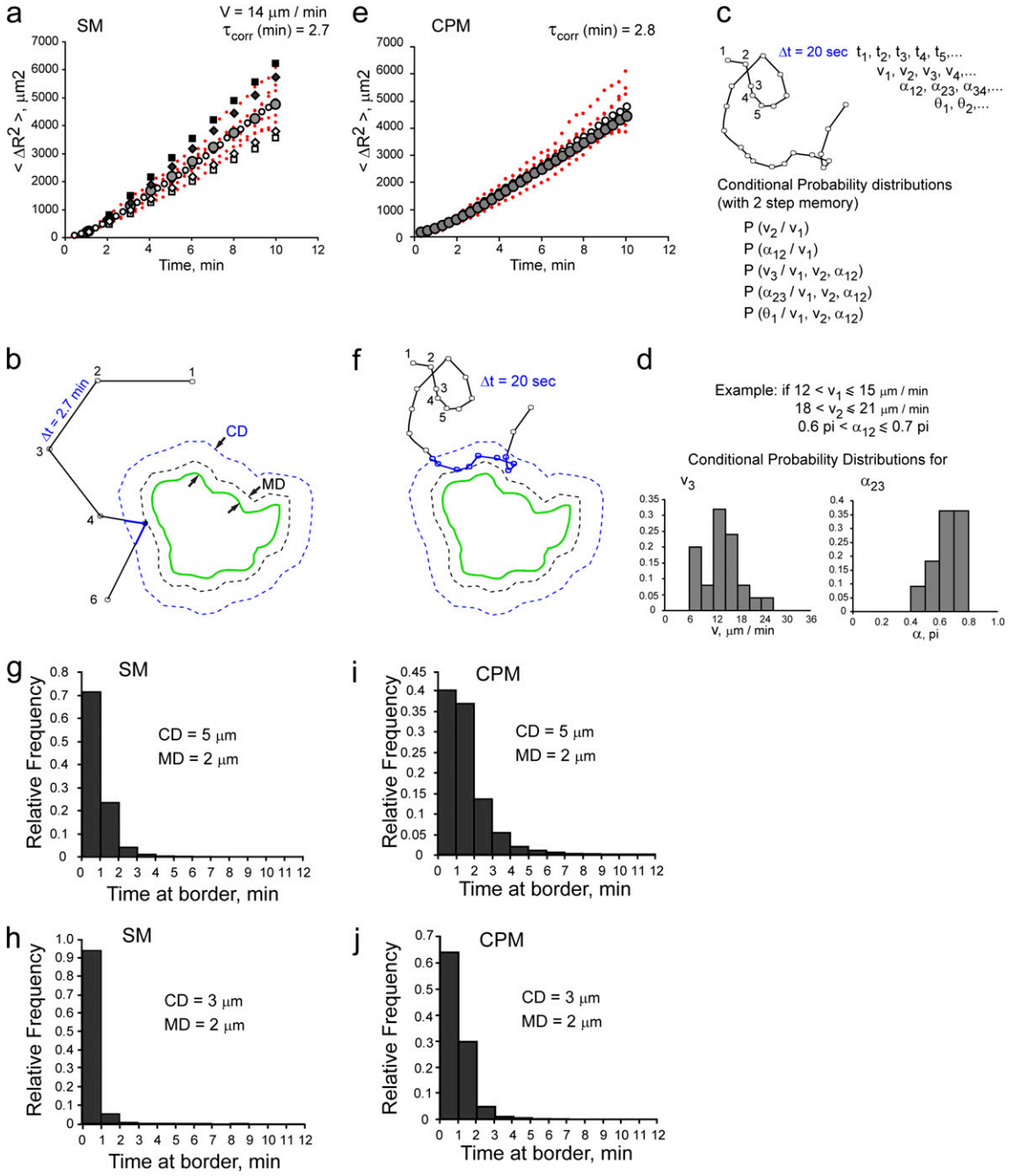

Fig. S6. Simple model (SM) and conditional probability model (CPM) algorithms for T-cell random walk within ILN. (*A*) Average squared displacement $<\Delta R^2>$ vs. time, calculated for T-cell migration in the T zones of explanted ILNs in six independent TPLSM experiments (red dots). White circles indicate the average $<\Delta R^2>$ vs. time for six experiments. Gray circles represent $<\Delta R^2>$ vs. time calculated from the random trajectories generated by SM with the period of straight motion Δt set to 2.7 min (equal to the average experimentally measured τ_{corr}) and velocity, V to 14 μm/min. Black and white squares represents $<\Delta R^2>$ vs. time calculated by the SM when Δt was fixed at 2.7 min and velocities V set to 16 and 12 μm/min correspondingly. Black and white diamonds represent $<\Delta R^2>$ vs. time calculated by the SM when velocity V was fixed at 14 μm/min and the period of straight motion Δt was set to 3.3 and 2.1 min correspondingly. (*B* and *F*) Schematics illustrating trajectories generated by the SM (*B*) or the CPM (*F*) algorithms in proximity to the in silico LYVE-1$^+$ sinuses (green). Black dashed lines outline MD to the sinuses, which cell trajectories cannot cross. In both algorithms a new random step is then generated that is at a greater distance to the LYVE-1$^+$ sinuses than the MD. Blue dashed lines outline the CD from the sinuses. When trajectories cross these lines they are registered as "in contact" with LYVE-1$^+$ sinuses (blue regions of the trajectories). (*C–E*) Development of the conditional probability model. (*C*) Example of T-cell trajectory. To build a conditional probability model of T-cell random walk, sequential (collected every 20 s) apparent velocities, v, angles, α, and plane angles, θ, were extracted from trajectories collected in six experiments (>60 tracks each, each track at least 10 min long). Using these sequences, conditional probability distributions for v, α, and θ were calculated that depended on the combinations of v and α in the preceding step(s) as described in *SI Materials and Methods*. Combination of the calculated conditional probabilities with a two (20 s)-step memory gave the best fit to the experimental data (*E*). (*D*) Illustration of the conditional probability distribution calculation principle. Frequency distributions for v_{i+1} and $\alpha_{i\ i+1}$ were collected from all analyzed trajectories, where two preceding sequential local velocities, v_{i-1} and v_i, and the angle between them $\alpha_{i-1\ i}$ lay within the indicated range. (*E*) $<\Delta R^2>$ vs. time calculated from the random trajectories generated by the CPM with the conditional probability combination indicated in *c* (gray circles). Red dots and white circles represent the same as in *a*. τ_{corr} of the trajectories generated by the CPM is 2.8 min. (*G–J*) Distributions of time spent by in silico T cells at the border of the LYVE-1$^+$ sinuses when calculated by SM (*G*, *H*) and CPM (*I*, *J*) algorithms, with minimal distance (MD) set to 2 mm and contact distance (CD) set to 5 mm (*G*, *I*) or 3 mm (*H*, *J*).

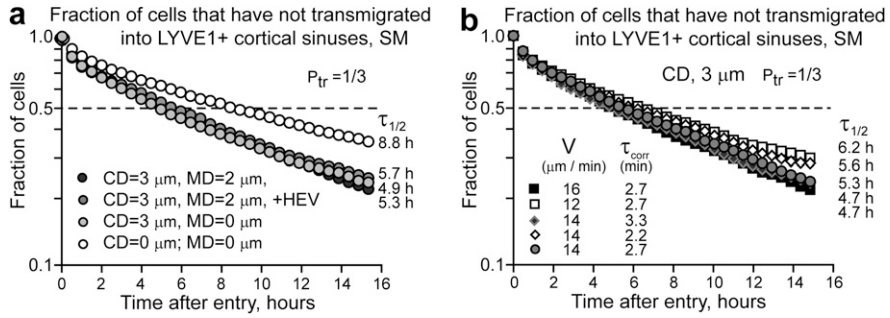

Fig. S7. Analysis of the SM sensitivity to parameter variation. (*A* and *B*) The fraction of cells that have not transmigrated into LYVE-1$^+$ sinuses (in silico), depending on the time after their entry into the LN, calculated by the SM algorithm. Half-life, $\tau_{1/2}$, indicates the time when half of the cells in silico transmigrate into sinuses. Transmigration efficiency is set to 0.3 and does not change with time. (*A*) Sensitivity of the SM to variation in CD, MD, and HEV avoidance. Black circles represent predictions of the SM for CD = 3 μm and MD = 2 μm. Light gray circles, CD = 3 μm and MD = 0 μm. White circles, CD = 0 μm and MD = 0 μm. Dark gray circles represent predictions of the SM with CD = 3 μm and MD = 2 μm, under conditions in which SM cell trajectories cannot approach HEVs closer than 2 μm during their random walk ILN. (*B*) Sensitivity of the SM to variation in speed and the time of correlated motion that results in changes in displacement, represented in Fig. S6*A*. CD = 3 μm and MD = 2 μm. Gray circles represent $<\Delta R^2>$ vs. time calculated from the random trajectories generated by the SM with the period of straight motion Δt set to 2.7 min (equal to the average experimentally measured τ_{corr}) and velocity, *V*, to 14 μm/min. Black and white squares, Δt fixed at 2.7 min and velocities *V* set to 16 and 12 μm/min correspondingly. Black and white diamonds, velocity *V* fixed at 14 μm/min and the period of straight motion Δt set to 3.3 and 2.1 min correspondingly.

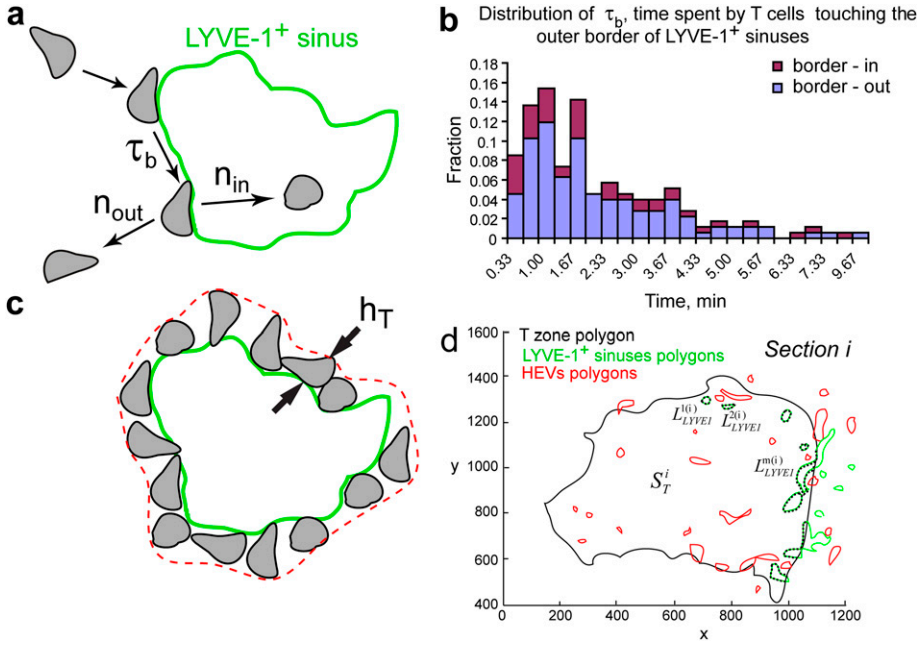

Fig. S8. Volumetric analysis. (*A*) A scheme indicating possible T-cell behaviors upon contact with LYVE-1$^+$ sinuses (outlined by green line). τ_b, time that T cells spend in contact with LYVE-1$^+$ sinus outer border before transmigration into the sinus or return back to parenchyma. (*B*) Experimentally measured distribution of τ_b for cells that move into LYVE-1$^+$ sinus after traversing the border (maroon bar, *n* of events, 45) or return into parenchyma (blue bar, *n* of events, 131). Calculation was from four independent TPLSM experiments, on the basis of the quantitative analysis of T-cell migration in relation to the cortical sinuses performed as described in *SI Materials and Methods* (1). (*C*) A scheme demonstrating T cells touching the outer surface of the LYVE-1$^+$ sinus (green line). Dashed line indicates the distances from the sinus wall, taken by LYVE-1$^+$ sinus touching T cells. h_T is the average of these distances in ILNs, suggested in the volumetric analysis to lie somewhere between 5 and 10 μm. (*D*) MatLab exported image of a single *z* plane (section *i*) of ILN with polygons outlining T zone (black), HEVs (red), and cortical sinuses (green). S^i_T, area of the T-zone polygon of section *i*. $L^{m(i)}_{LYVE1}$, perimeter of the *m*th LYVE-1$^+$ sinus polygons in section *i*, facing the T zone (within T-zone polygon), outlined by black dots.

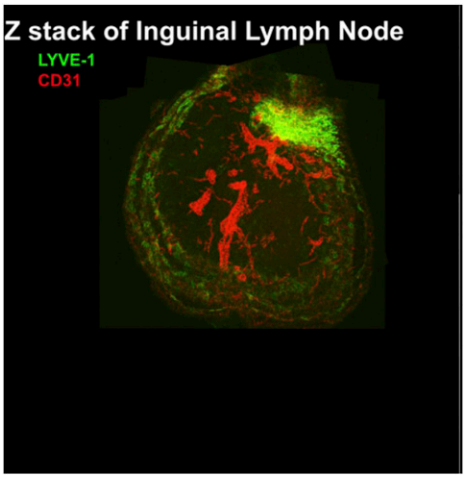

Movie S1. *Z* stack of inguinal lymph node (ILN). Z stack of a three-dimensional (3D) reconstruction of an ILN is shown in the direction from the cortical side toward the medulla, obtained by ILN serial sectioning, followed by staining of the sections with antibodies specific for LYVE-1 (green), CD31 (red), and CD4 (not shown) and imaging by confocal microscopy. LYVE-1-specific antibody stained cortical, medullary, and subcapsular (SCS) sinuses, as well as reticular cells and macrophages in the medullary region. MR, medullary region between the two lobes of the ILN. Each plane of the *z* stack shows a 45-μm-thick projection view of the serial confocal sections. One hundred units (between major tick marks) correspond to 146 μm. Overall thickness of the reconstruction is ~575 μm. Examples of blunt-ended and intermediate cortical LYVE-1$^+$ sinuses are indicated with arrows.

Movie S1

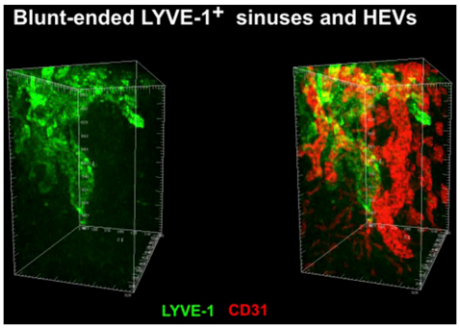

Movie S2. Proximity between blunt-ended cortical sinuses and HEVs. The movie shows a 3D view of two blunt-ended cortical LYVE-1$^+$ sinuses in relation to HEVs. 3D reconstruction was obtained by ILN serial sectioning, followed by staining for LYVE-1 (green) and CD31 (red) and imaging by confocal microscopy. The left view shows LYVE-1 alone and the right view the combination of LYVE1 with CD31. Major tick marks correspond to 20 μm.

Movie S2

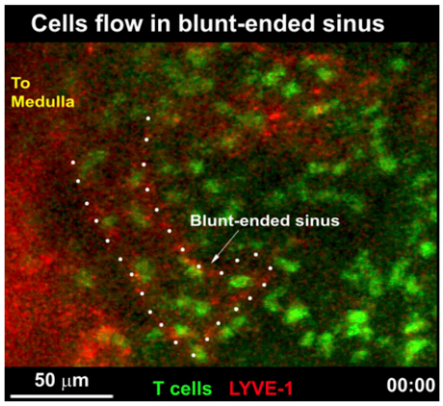

Movie S3. T-cell flow in a blunt-ended cortical sinus. Intravital TPLSM is shown of an ILN with transferred GFP$^+$ T cells (green) and labeled with Texas Red-conjugated anti-LYVE-1 (red). The time-lapse image sequence shows a 12-mm-thick *z* projection of a blunt-ended LYVE-1$^+$ cortical sinus outlined by white dots. The blunt-ended nature of the sinus was confirmed by *z*-stack analysis. A few rapidly moving cells that appear to cross the sinus are out-of-focus projections of the cells from other *z* stacks. Elapsed time is shown as min:s.

Movie S3

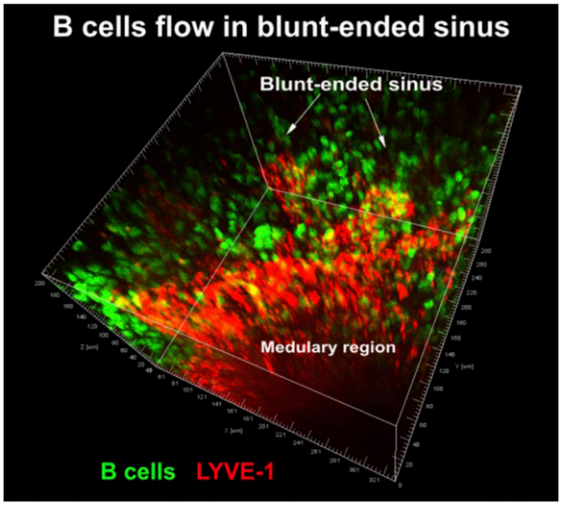

Movie S4. B-cell flow in a blunt-ended cortical sinus. Intravital TPLSM is shown of an ILN with transferred GFP$^+$ B cells (green) and labeled with Texas Red-conjugated anti-LYVE-1 (red). The first image sequence shows a 3D view of an ILN region visualized by TPLSM. The square outlines the blunt-ended LYVE-1$^+$ sinuses region where cell migration was analyzed by tracking analysis. The next image sequence zooms in on the outlined region and shows rotational views of the 3D image with rendered blunt-ended structures and B-cell trajectories. Tracks in various colors represent trajectories of B cells that enter the blunt-ended sinuses. The final segment of the movie is a 30-min time-lapse sequence showing movement of the B cells (represented by spheres that indicate center of B-cell coordinates) along these trajectories. White triangles indicate entry of B cells into the blunt-ended sinuses from parenchyma. Yellow triangles indicate return of B cells from the sinuses back to the outer surface of the sinuses or into the parenchyma. Elapsed time is shown as min:s.

Movie S4

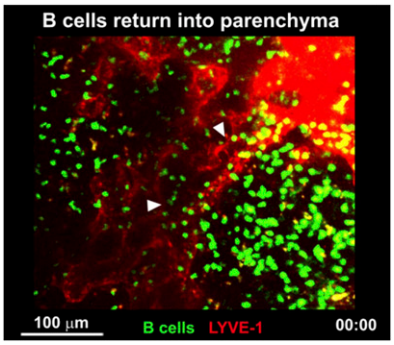

Movie S5. B-cell return from LYVE-1$^+$ sinuses into parenchyma. Intravital TPLSM is shown of an ILN with transferred GFP$^+$ B cells (green) and labeled with Texas Red-conjugated anti-LYVE-1 (red). The first time-lapse image sequence shows a 21-mm-thick *z* projection of a network of cortical LYVE-1$^+$ sinuses connected to the capsule. The white arrowheads indicate the regions of flowing B cells that were subjected to B-cell tracking analysis. The next image sequence shows volume rendering of the regions and tracks of the B cells that got out of the sinus and returned back into the parenchyma. The following movie shows movement of B cells (represented by green spheres that indicate the center of B cell coordinates) inside (dim signal) and outside (bright colors) of these sinuses. Elapsed time is shown as min:s.

Movie S5

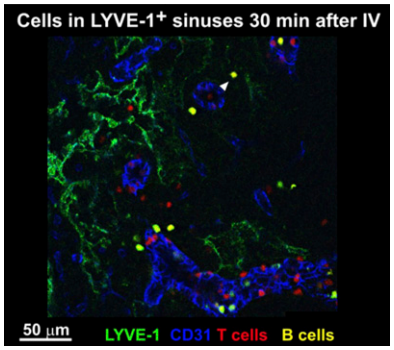

Movie S6. Confocal reconstruction showing cells in cortical sinuses 30 min after i.v. transfer. *Z* stack is shown of confocal images of the peripheral lymph node sections from mice, i.v. injected for 30 min with T cells, labeled with CMTMR (red), and B cells, colabeled with CMTMR and CFSE (yellow) and stained with LYVE-1-specific antibody (green) and CD31-specific antibody (blue). Thickness of the *z* stack is 16 mm.

Movie S6